BUTTERWORTH HEINEMANN

Contouring algorithm for ion figuring

Thomas W. Drueding,* Thomas G. Bifano,* and Steven C. Fawcett†
*Aerospace and Mechanical Department, College of Engineering, Boston University, Boston, MA, USA; and †Optical Fabrication Branch, EB53, National Aeronautics and Space Administration, Marshall Space Flight Center, AL, USA

Ion beam figuring provides a highly deterministic method for the final precision figuring of optical components with advantages over conventional methods. The ion-figuring process involves bombarding a component with a stable beam of accelerated particles, which selectively removes material from the surface. The specific figure corrections are achieved by rastering the fixed-current beam across the workpiece at varying velocities. Unlike conventional methods, ion figuring is a noncontact technique that avoids such problems inherent in traditional fabrication processes as edge roll-off effects, tool wear, and force loading of the work piece. Other researchers have demonstrated that ion beam figuring is effective for correcting of large optical components. This work is directed toward the development of the precision ion-machining system (PIMS) at NASA's Marshall Space Flight Center (MSFC). This system is designed for processing small (≅10 cm diameter) optical components. The ion-figuring process involves obtaining an interferometric error map of the surface, choosing a raster pattern for the beam, and determining the velocities along that path. Because the material removed is the convolution of the fixed ion beam removal and the rastering velocity as a function of position, determining the appropriate velocities from the desired removal map and the known ion beam profile is a deconvolution *process. A unique method of performing this deconvolution was developed for the project, which is also applicable to other mathematically similar processes, including computer-controlled polishing. This paper presents the deconvolution algorithm, a comparison of this technique with other methods, and a simulation analysis. Future research will implement this procedure at MSFC.*

Keywords: *ion figuring; optical fabrication; deconvolution*

Introduction

The figuring step in the fabrication of an optical component involves imparting a specified contour onto the surface. This can be expensive and time consuming. The recent development of ion beam figuring provides a method for performing the figuring process that has advantages over standard mechanical methods. Ion figuring has proved to be effective in figuring large optical components.[1–7]

Address reprint requests to T. G. Bifano, Aerospace & Mechanical Department, Boston University, 110 Cummington St., Boston, MA 02215, USA.

The process of ion beam figuring removes material by transferring kinetic energy from impinging neutral particles. The process utilizes a Kaufman-type ion source, where a plasma is generated in a discharge chamber by controlled electric potentials.[8] Charged grids extract and accelerate ions from the chamber. The accelerated ions form a directional beam. A neutralizer outside the accelerator grids supplies electrons to the positive ion beam. It is necessary to neutralize the beam to prevent charging workpieces and to avoid bending the beam with extraneous electromagnetic fields. When the directed beam strikes the workpiece, material sputters in a predicable manner. The amount and distribution of material sputtered is a function

Precision Engineering 17:10–21, 1995

655 Avenue of the Americas, New York, NY 10010
0141-6359/95/$10.00
SSDI 0141-6359(94)00002-H

of the energy of the beam, material of the component, distance from the workpiece, and angle of incidence of the beam. The figuring method described here assumes a constant beam removal, so that the process can be represented by a convolution operation. A fixed beam energy maintains a constant sputtering rate. This temporally and spatially stable beam is held perpendicular to the workpiece at a fixed distance. Correction would have to be made for nontemporally or spatially constant removal to model the process by a convolution operation. Specific figures (contours) are achieved by rastering the beam over the workpiece at varying velocities.

Prior to any machining, a *beam function* must be determined for the system. The beam function, analogous to a point spread function, provides a depth removal rate as a function of radial distance from the beam center. The ion-figuring process begins with interferometrically measuring the contour on the workpiece, resulting in an x–y array map of relative surface height values. A *removal map,* the difference between the measured surface contour and a desired surface contour, describes the material to be removed. From the removal map and the beam function, a *dwell function* or map is calculated. The dwell function provides velocities used by a targeting program to control beam motions. For figuring, the component is placed in the machining apparatus, and the beam is rastered over the surface according to the dwell function. The material removed is represented by the convolution of the beam function and the dwell function. In NASA–MSFC's precision ion-machining system, the ion beam is held fixed and the workpiece is moved under the beam using x, y, and θ, motion, but for purposes of discussion we refer to moving the beam across the workpiece; this involves a simple change in the frame of reference.

Early work on the ion-figuring of optical components was performed by Gale.[9] This work was expanded at the University of New Mexico by Wilson et al.[5–7] Their initial experiments involved figuring of 30-cm fused silica, Zerodur, and copper optics with a 2.54-cm ion beam source. Allen et al. developed an ion-figuring system for large optics at Eastman Kodak.[1–4] The Kodak Ion-Figuring System (IFS) is capable of processing components up to 2.5 m $\times$ 2.5 m using several ion sources of up to 15-cm diameter. Other current research is being carried out at Oak Ridge National Laboratory. Their system is capable of figuring up to a 60-cm component.[10] The new PIMS research facility at NASA's Marshall Space Flight Center is focused on the figuring of small ($\cong$10-cm diameter) optics using a 3-cm ion source. Figuring smaller optics is difficult because the ratio of the beam width to the size of the component is greater. The algorithm presented in this paper was developed primarily to overcome some of the problems associated with the ion figuring process.

The two main advantages of the ion-machining process are that it is noncontacting and highly predictable. The noncontact nature eliminates the problems of tool wear and edge effects encountered in most standard polishing techniques. The process also avoids rib structure print through and warping caused by loading stresses on the workpiece. Holding beam parameters constant ensures beam stability and results in a predictable and highly deterministic removal process. This allows for rapid convergence of the process to required specifications, resulting in a significant time and cost savings. The addition of in-process metrology can increase the effectiveness and is possible because the method is noncontact, and an occluding machining tool is not present. It is also possible to combine the figuring with a coating process in the same vacuum chamber; better coating adhesion is expected from the clean surface left from ion machining. With a broad ion beam removal and the smoothing nature of a convolution, only smooth continuous contours can be imparted on the surface with this technique. This constraint is acceptable for producing most optics.

Issues of concern in ion beam-figuring process include; beam stability, the surface properties of the workpiece, workpiece heating, and dwell function computation. Beam stability affects the predictability and accuracy of the removal process, while workpiece surface properties and heating influence the effectiveness of the process. The effects on the surface roughness are reported in earlier work.[11]

A significant step in the process is the calculation of the dwell function that controls the rastering velocity. Because the ion beam-figuring process is a convolution process, the calculation of the dwell function is a deconvolution process. Difficulties in performing the deconvolution are accentuated in the processing of smaller optics because the scale of the workpiece is closer to the width of the ion beam (i.e., the computations involve a wider filter). A solution method for this problem is developed and discussed in the next section. The calculation of rastering velocities (dwell function) is independent of the x–y plane geometry of the workpiece. The algorithm requires information only on the actual surface geometry.

Algorithm

Figuring process

In the figuring process, the ion beam moves across the optical component. The parameters controlling the ion beam current are maintained constant and the beam source is held a fixed distance, perpendicular to the workpiece. Because the beam re-

moves material over a broad area, the removal process is a convolution of the ion beam's removal profile (the beam function) and the rastering velocity as a function of position (the dwell function). Determining the appropriate rastering velocities from the desired removal map and the known ion beam removal profile is therefore a *deconvolution* process. The actual figuring is done by one of two methods: 1) varying the speed of the ion beam as it is moved across the component; or 2) placing the beam at grid points for various periods of time. The PIMS rasters in concentric circles around the workpiece center. The velocity is then varied throughout each circular path to provide nonaxially symmetric corrections.

Prior to machining, the ion beam removal function must be characterized. The beam function is analogous to the filter or point spread function of the machining process. The function gives a removal rate at a point and has dimensions of length divided by time. The beam function is characterized by its shape and its intensity. The shape remains constant for a specific physical configuration of the apparatus and need only be determined once for that configuration. The beam function is roughly Gaussian shaped, as depicted in *Figure 1.* The intensity is dependent on the power supplied and the workpiece material, and it must be determined for each material.

The first step in a specific machining process is determining the desired removal map for the process. This corresponds to a map of the corrections necessary to the surface, and it is computed by subtracting the desired contour from the measured surface map provided by the metrology.

Problem formulation

The figuring process is represented in Equation (1) as a convolution where the asterisk represents the convolution operator. The convolution equation is used to represent many different processes, and is shown here with ion figuring variables.

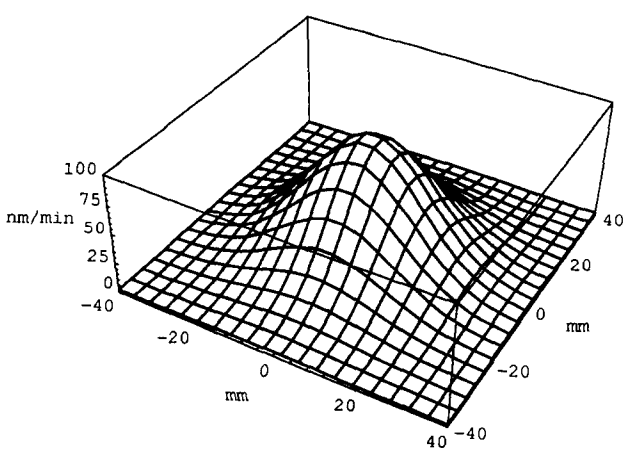

Figure 1 Gaussian modeled machining profile of 3-cm ion source

$$R(x,y) = \int_{-\infty}^{\infty}\int_{-\infty}^{\infty} B(x-u, y-v)\, T(u,v)\, du\, dv = B(x,y) * T(x,y) \quad (1)$$

The beam function B is a measure of the depth of material removed per unit time at a location relative to the beam center. The dwell function T represents the rastering velocity of a strip per unit width or the time the beam spends at a location on the workpiece per unit area. The convolution of the beam function and the dwell function is a surface of material removed from the workpiece R, the removal function. The properties of the functions are outlined in *Table 1.*

A dimensional representation of Equation(1) is shown in Equation (2) for clarity.

$$[L] = \int_{-\infty}^{\infty}\int_{-\infty}^{\infty}\left[\frac{L}{T}\right]\left[\frac{T}{L^2}\right] d[L]\, d[L] \quad (2)$$

This equation demonstrates that the dwell function has the units of time over length squared. The dwell function can now either be broken into areas and interpreted as a time, or it can be broken into strips and interpreted as a velocity. If the work space is broken into areas, each area has a time associated with it. This is the amount of time the beam must be positioned in that area and is equal to the integral of the dwell function over the area. For example, if the total workspace is broken into a square grid, the beam is centered at each square an amount of time approximately equal to the value of the dwell function at the center times the area of the square.

$$\text{dwell time at } i,j = \int\int_{A_{ij}} T(x,y)\, dx\, dy \cong T(u_i, v_j)\, \Delta u\, \Delta v \quad (3)$$

This method discretizes Equation (1).

$$R(x,y) = \sum_{i=0}\sum_{j=0} B(x-u_i, y-v_j)\, T(u_i, v_j)\, \Delta u\, \Delta v \quad (4)$$

The optical component's surface profile and therefore the removal functions are provided as an x–y grid array from the metrology equipment. This discretization of the removal function suggests discretizing the figuring process in the same manner because the process is then exactly a square dis-

Table 1 Function definitions and properties

Definition	Symbol	Dim	Units
Removal function	R	$[L]$	nm
Beam function	B	$[L/T]$	nm/s
Dwell function	T	$[T/L^2]$	s/mm^2
Surface units	x, y, u, v	$[L]$	mm

crete convolution. The calculations, then, maintain the same discretization as the metrology equipment. During figuring, the rastering pattern either must be constrained to the discretization of the metrology or approximated from this grid.

Alternatively, the workspace is broken in strips, where each strip has a width and a velocity function associated with it. The velocity function is the speed that the beam is rastered along the strip, and it is equal to the inverse to the inverse of the dwell function integrated over the strip width.

$$V(x,y) = \frac{1}{\int_s T(x,y)\, ds} \tag{5}$$

For example, the figuring process in Equation (1) with partial Cartesian discretization is approximated as follows.

$$R(x,y) = \sum_{i=0} \int_{-\infty}^{\infty} B(x - u, y - v_i)\, T(u,v_i)\, du\, \Delta v \tag{6}$$

Each one-dimensional strip has a characteristic width. For example, if the workspace is broken into strips parallel to the x-axis, the width is the y separation between the boundaries of the strips.

$$V(x) \cong \frac{1}{T(x,y_i)\, \Delta y} \tag{7}$$

The PIMS uses polar coordinates and forms strips with concentric circles, each having a characteristic width of Δr. The tangential velocity is used here.

$$V(\theta) \cong \frac{1}{T(r_i,\theta)\, \Delta r} \tag{8}$$

Another method considers a spiral strip from the center of the workpiece. This provides one strip to cover the entire piece. This has not been done because of the difficulties in coordinating the translational and rotational axes.

The strip–velocity method provides a partial discretization that has some advantages over the area–time method, and it is a more eloquent operation. It is common in the area–time method that the beam remains on while the beam transverses from one grid point to another. This causes unwanted removal if the positioning time is not negligible compared to the dwell time in an area. In the Cartesian strip–velocity method, the rastering function is continuous and strip positioning is done off the workpiece so that there is no extraneous material removal. Another advantage is that one level of discretization has been removed since the solution is not based on the discretization of the metrology. Although the translating motion may have its own inherent discretization, this discretization is usually smaller than that of the metrology, and it is possible to control the velocity or acceleration to attain a higher order of accuracy.

Historical methods

Early work by Wilson et al. at the University of New Mexico on the figuring of optical components uses Fourier transform techniques to solve for a dwell time function.[5–7] In that technique, the convolution operation in Equation (1) is represented in the frequency domain by Fourier transformation as a multiplication.

$$\tilde{R} = \tilde{B}\tilde{T} \tag{9}$$

The deconvolution simply involves dividing by the beam function (filter) and taking the inverse Fourier transform of the result.

$$T(x,y) = \mathfrak{F}^{-1}\{\tilde{R}/\tilde{B}\} \tag{10}$$

The authors report two specific difficulties with obtaining this solution. First, the integration in Equation (10) is unstable and has particular difficulties where the Fourier transform of the beam removal function approaches zero. For example, consider the one-dimension continuous case, where the beam removal function is a Gaussian function, $B(x) = \exp[-x^2]$, the transform is $\tilde{B}(k) = \exp[-k^2/4]$, and so the Fourier integral represented by Equation (10) is divergent because the negative power becomes positive in dividing by $\tilde{B}(k)$.

$$T(x) = \frac{1}{2\pi} \int_{-\infty}^{\infty} e^{-ikx}\, e^{k^2/4}\, \tilde{R}(k)\, dk \tag{11}$$

This is resolved using a thresholded inverse filter. Another problem in the computation arises from the discretization. The computations are performed using discrete Fourier transforms, which demand that the inputs be periodic on finite x–y arrays with the same dimensions. Although the metrology provides a rectangular array of surface heights, the optical component itself does not necessarily fill that array. A point in the array outside the workpiece must be filled with some value (often zero). The method still accounts for those areas in the computation and will provide a solution partially directed toward figuring areas that are nonexistent. The problem is addressed by using a band limited surface extrapolation (BLSE) process to construct data in the missing areas. BLSE is a method for recovering information from partial or incomplete data.

In another implementation, the Kodak IFS uses an iterative solution.[4,12] The iterative method for finding a solution to the dwell function should not be confused with the idea of iterating the entire ion-figuring process to make further corrections. A first guess for the dwell time function is made (possibly equal to the rescaled desired removal function) and used for computing the convolution. The result is used to make corrections for a new solution. The computation is then iterated several times until the predicted error is sufficiently small. A simplified iterative equation is shown here where k

represents a relaxation factor (similar to the feedback process gain in a control loop).

$$T_{n+1} = T_n + k(R - B * T_n) \tag{12}$$

In this system, the computations are performed using x–y arrays, and the machining process involves rastering the beam over strips. Velocity values must be interpolated from the resulting x–y grid. In the machining of the hexagonal Keck segment an 8th order (45-term) Zernike polynomial fit was used to the original surface data.[3] This allows the computations at any discretization but assumes that the fit sufficiently characterizes the surface. The fit also fills in areas where the optical component does not exist. Iterative methods are not always stable and do not always converge to a unique answer.[12]

At Oak Ridge National Labs, a matrix algebraic approach is used to solve for the dwell function map array.[10] The method requires that an inverse matrix to a beam function map be computed. The problem is the matrix for the beam function is sparse and highly singular. Single valued decomposition (SVD) methods are used to construct the solution. Most traditional deconvolution methods used in the ion-machining process utilize the discretization of the metrology in all computations. An x–y grid dwell time map is provided from the metrology (typically interferometry) and must be followed. Additionally, in these techniques, it is difficult to account for, or allow, figuring effects outside the computation/metrology grid system. The following solution performs an approximation before the computation of the dwell function. In practice, all deconvolution methods and variations do not necessarily provide the same answers. Different answers may even be encountered for different computational parameters or numerical accuracies.

Series solution method

The algorithm used for the PIMS is based on a series solution technique. The process of getting from a series expansion for the known removal function to a series expansion for the unknown dwell function is shown first. The methods for computing the necessary conversion coefficients are also shown. In the following section, the operational steps are outlined.

The solution to convolution Equation (1) can be expressed in terms of derivatives of the known function and inverse moments of the filter.[13,14]

$$T(x,y) = \sum_{p=0}^{\infty}\sum_{q=0}^{\infty}\beta_{pq}\,\nabla^{pq}\,R(x,y) \tag{13}$$

The derivative operator is defined as $\nabla^{pq} = \partial^p{}_x\partial^q{}_y$. The weighted statistical moments of the beam function are used to calculate the inversion coefficients. The beam function must have finite moments. The weighted moments of the beam function (the filter) are defined as follows.

$$\alpha_{pq} = \frac{(-1)^{pq}}{p!q!}\int_{-\infty}^{\infty}\int_{-\infty}^{\infty} x^p\,y^q\,B(x,y)\,dx\,dy \tag{14}$$

The inversion coefficients are determined by inverse series algebra (Bochner algebra).[15]

$$\beta_{00} = 1/\alpha_{00}$$

$$\beta_{ij} = -\beta_{00}\sum_{p=1}^{i}\sum_{q=1}^{j}\beta_{(i-p)(j-q)}\,\alpha_{pq}\quad i,j \neq 0 \tag{15}$$

The desired removal function is actually only known at a number of arbitrary points located anywhere within the space, and it represents the shape of the workpiece in the x–y plane. An area where the piece does not exist is not relevant to the computation of the dwell function but can be relevant in the use of the dwell function. A function can be fit (more specifically a series expansion) to the known data points without regard to the discontinuities or unknown areas. An assumption is made that the expansion sufficiently represents the data. The removal function $R(x,y)$ is represented here as a linear combination of general $k \times k$ basis functions $\phi_{lm}(x,y)$. The parameters or expansion coefficients a_{lm} are determined by standard linear least squares fitting.[16]

$$R(x,y) = \sum_{l=0}^{k}\sum_{m=0}^{k} a_{lm}\phi_{lm}(x,y) \tag{16}$$

The removal function in Equation (16) is defined over all space and is substituted into the solution for $T(x,y)$ of Equation (13). Because the expansion coefficients are independent of the location, they are brought outside the derivative operator.

$$T(x,y) = \sum_{p=0}^{\infty}\sum_{q=0}^{\infty}\sum_{l=0}^{k}\sum_{m=0}^{k}\beta_{pq}\,a_{lm}\,\nabla^{pq}\phi_{lm}(x,y) \tag{17}$$

The basis functions can represent any expansion, but are specifically defined here as separable weighted polynomials in x and y.

$$\phi_{ij}(x,y) \equiv \phi_i(x)\phi_j(y) \qquad \phi_i(x) = \frac{x^i}{i!} \tag{18}$$

These basis functions are chosen because they have the property that the nth derivative of the ith basis function is the $(i - n)$th basis function, until the zero'th order (i.e., all negative order basis functions are zero)

$$\nabla^n\,\phi_i(x) = \phi_{i-n}(x) \tag{19}$$

This allows the substitution for the derivative operator in Equation (17), and the infinite series automatically truncates at k.

$$T(x,y) = \sum_{p=0}^{k}\sum_{q=0}^{k}\sum_{l=0}^{k}\sum_{m=0}^{k} \beta_{pq}\, a_{lm}\, \phi_{(l-p)(m-q)}(x,y) \tag{20}$$

By substituting $i = l - p$ and $j = m - q$, an expression for $T(x,y)$, the dwell function, is found with the identical form as the expansion for $R(x,y)$.

$$T(x,y) = \sum_{i=0}^{k}\sum_{j=0}^{k} b_{ij}\, \phi_{ij}(x,y) \tag{21}$$

The coefficients of the dwell function (b_{ij}) are defined by the following.

$$b_{ij} = \sum_{l=i}^{k}\sum_{m=j}^{k} a_{lm}\, \beta_{(l-i)(m-j)} \tag{22}$$

This method provides a very efficient and exact solution of the expansion of $R(x,y)$ for the convolution Equation (1). The only assumption is that the original removal surface is polynomic in nature and is sufficiently represented by the expansion of order $k \times k$. There is no special consideration for the geometry of the workpiece in the x–y plane. The solution is represented by a function that provides values over the entire space for controlling the beam. The only computationally intensive operation is the fitting of the expansion in Equation (16). The higher the order of the expansion k, the more accurate the solution becomes, but the longer the computations take. The fitting process may also get unstable for very high-order polynomials because the linear equations become close to singular. The accuracy of the original fit provides a measure of how well the process can be expected to perform and can easily be checked prior to machining. Because of errors in the actual machining process and the limitations of the metrology data, there will be a saturation limit where increasing the order of the expansion will no longer improve machining accuracy. In the final analysis of the following section, it is demonstrated that expansions of moderate order containing only 15 terms is sufficient for practical machining operations. For the PIMS process, the expansion order will be chosen to achieve a specified accuracy.

The solution and algorithm are applicable to solving many problems that can be represented by the convolution equation, including computer controlled polishing.

Step-by-step procedure

This section describes the operational algorithm for using the derivative-series solution. This has been implemented in C++ and integrated into the PIMS control program. The Analysis section describes some of the initial testing and verifying done. A map of surface heights on the optical component is the primary input, together with a target figure contour. The program then provides a dwell function for controlling the rastering of the ion beam. The procedure used in the process is outlined below.

1. *Calculate inversion coefficients:* Prior to machining, the moments of the beam removal function are determined. The inverse coefficients are computed from the moments, as outlined in the series solution section. The moments can be determined directly from data or analytically from a functional form of the beam. Any function with finite moments can be used for the beam function.

   The PIMS assumes a Gaussian beam function $B(x,y) = \Gamma\ \mathrm{Exp}[-(x^2 + y^2)/\omega^2]$. The inverse coefficients are given as follows:

   $$\beta_{pq} = \frac{(-1)^{p+q/2}}{\Gamma\pi\omega^2}\frac{(\omega/2)^{p+q}}{(p/2)!(q/2)!} \qquad p,q \ \text{ even} \tag{23}$$

   For even functions, only the even moments exists; therefore, only even inverse moments exist. Thus, in the Gaussian function used for the ion beam profile, the odd inverse coefficients are zero. The parameter Γ is the peak material removal rate, and the parameter ω represents the width of the beam function. These two parameters completely characterize the Gaussian beam function.
2. *Load surface map:* An interferonmetric map of the optical component's surface height data is loaded in an array, *sample map.* Included in the surface height data is a coordinate system for the x–y location and information on which points represent real data and which points are invalid.

   $$S_{ij} \text{ at } x_i, y_j \tag{24}$$

   In the PIMS, a ZYGO Mark IV interferometer is used to measure the surface heights. The relative location of the data points is determined by dividing the known diameter of a circular workpiece by the number of points across the surface map
3. *Subtract desired contour map:* The material to be removed, the *removal map* (R_{ij}), is equal to the surface map minus a desired surface contour map $C(x,y)$. This can be considered an error map of surface features.

   $$R_{ij} = S_{ij} - C(x_i, y_j) \tag{25}$$

4. *Fit removal function:* The removal map is now fit to a series expansion. The order of the fit must be chosen at this step. The problem of finding the fitting coefficients is posed as a linear problem by setting up a one-dimensional array equal to the number of actual data points in the x–y removal map and

following standard linear least-squares routines.

$$R(x,y) = \sum_{l=0}^{k} \sum_{m=0}^{k} a_{lm}\, \phi_{lm}(x,y) \tag{26}$$

The accuracy of the expansion is checked to ensure that it sufficiently represents the difference between the surface map and the desired contour map. This accuracy is determined by the root-mean-square (rms) difference between the removal map and the computed removal function expansion η, defined below as the *goodness-of-fit* measure.

$$\eta = \sqrt{\sum_i \sum_j (R_{ij} - R(x_i,y_j))^2/N} \tag{27}$$

The summation is performed only over existing data points where N is the total number of actual data points. The figuring process will not make the resulting surface any closer to the desired contour than the accuracy of this fit. We use modified routines taken directly from a standard numerical text.[16]

5. *Deconvolve:* The deconvolution is performed by using the solution for the coefficients of the dwell function as calculated from the coefficients for the removal function and the inverse moments of the beam function.

$$b_{ij} = \sum_{l=i}^{k} \sum_{m=j}^{k} a_{lm}\, \beta_{(l-i)(m-j)} \tag{28}$$

After the deconvolution is performed, the constant term in the expansion is adjusted to ensure that the dwell function is positive within the workarea. This is done by checking grid points within the workarea and subtracting the lowest value from the constant term. This is also done to provide the solution with the lowest total dwell time.

The algorithm results in the coefficients for the dwell function that are used to control the motion of the ion beam during the actual machining process.

$$T(x,y) = \sum_{i=0}^{k} \sum_{j=0}^{k} b_{ij}\, \phi_{ij}(x,y) \tag{29}$$

The workarea is now broken into strips with a characteristic width. For each strip, the ion beam is moved along the center of the strip at velocities determined as in the Problem Formulation section. At the end of the current strip, the beam is repositioned for the subsequent strip. After the operation is complete, the resulting surface figure of the optical component is measured again. The quality of the optical component's contour is determined as the rms deviation between the surface and the desired contour.

$$\zeta = \sqrt{\sum_i \sum_j (S_{ij} - C(x_i,y_j))^2/N} \tag{30}$$

Again, the sum is only over datapoints that exist, and N is the total number of points. The initial quality is the deviation from the original surface ζ_i, and the final quality is the deviation from the postmachining surface ζ_f. The final rms difference between the resulting final map surface and the desired contour map will be no better than the goodness-of-fit measure (the rms difference between the removal function fit to the removal map) $\zeta_f \geq \eta$. The difference between the initial and final rms surface figure is the improvement achieved by the figuring process.

Analysis

Processing models

Models of the ion-machining process were developed to identify critical parameters, to establish theoretical limits of the operation, and to evaluate the deconvolution algorithms prior to machining experiments. Simulations modeling the operation of rastering the beam across the workpiece are represented by a discrete convolution. The simulations utilize data obtained from an actual optical sample 60-mm in diameter, as measured on a ZYGO Mark IV interferometer. The process modeled imparting both an ideal flat and a spherical contour on the sample workpiece. The simulations were not designed to predict the system exactly but to provide relative information. The simulations indicated those parameters to which the process is sensitive, not the precise reaction to the particular parameters.

The main objective of this analysis is to evaluate the necessary or optimal values for the process variables before machining is performed. During the deconvolution process, the order of the functional fit to the removal map k is the primary operator supplied variable. The effects of this order on predicted performance are shown. Also, the sensitivity to particular types of error are explored to provide information on the necessary positioning accuracy of the optical component. An understanding is achieved on how fluctuations or inaccuracy in beam function contribute to errors in the process. Another important objective is to understand the theoretical limits of the ion machining system given the modeled errors.

The simulations compute the convolution operation as a discrete convolution where s_g, s_h represent the coordinate systems of the convolution model's discretization, and Δr is the separation.

$$R(x_i,y_j) = \sum_{g=0} \sum_{h=0} B(x_i - s_g, y_j - s_h)\, T(s_g,s_h)\, \Delta r\, \Delta r \tag{31}$$

The metrology dictates the coordinate system of the removal function x_i and y_j. The resulting removal map is then subtracted from the original surface data to provide the theoretical postprocessing surface map. The accuracy of the figure of an optical component is quantified as the rms difference between the surface map and the desired contour map ζ, as defined in the previous section. Therefore, the measure of the effectiveness of the process is the difference in the initial and final rms deviation. The parameter available when determining the solution to the dwell function is the order of the fit k. For initial experiments, the solution determined has $k \times k$ terms in the expansion in Equation (16). The fit to the desired removal is an expansion of the same order, and the accuracy of the fit is a measure of what can be expected during the actual processing. The effects of higher-order k on the original fit and on the simulated removal is explored later.

The beam function is modeled as a Gaussian for the simulation and the solution is defined in Equation (32) and shown in *Figure 1.*

$$B(x,y) = \Gamma e^{-(x^2+y^2)/\omega^2} \tag{32}$$

For the simulations, a beam width of $\omega = 10$ mm is chosen based on previous beam data for determining the solution. This roughly corresponds to the expected shape of the 3-cm source in the actual ion machining apparatus. Larger sources will not be used, but it may be possible to narrow the beam by placing a small aperture in the path of the accelerated ions. This would reduce the width of the beam and the overall beam shape, but the peak removal should remain unchanged. The solution assumes a constant peak removal of $\Gamma = 100$ nm/min. The volumetric removal rate is a function of the two parameters.

$$\gamma = \Gamma \pi \omega^2 \tag{33}$$

This results in a volumetric removal rate $\gamma = 0.0314$ mm^3/min for the simulations. The data array used is 66×66 for a total of 4,356 locations but there are data at only 3,384 locations because of the circular nature of the component and drop-out spots from the interferometry. The separation between each data point is approximately 0.9 mm. The simulations involve the figuring of the optic to an ideal flat and to a sphere of 400-m radius. The current figure deviates 234 nm rms from flat, and the deviation from the sphere is 114 nm rms. The discretization of the convolution ΔR is chosen at 1.0 mm.

Error models

The figuring system is subject to inherent processing errors; their respective sensitivities need to be determined. All the errors modeled here are realized through the beam function, but they can represent such other errors in the system as inaccurate positioning of the workpiece on the translation stage. The simulated errors are introduced as variations in the beam function parameters and the relative positioning of the beam. Systematic offset errors and normally distributed random errors in the parameters are instituted by adjusting the variables in the beam function of Equation (32).

$$\begin{aligned} \omega &= \omega_0 + \omega_{off} + \sigma_\omega N \\ \Gamma &= \Gamma_0 + \Gamma_{off} + \sigma_\Gamma N \\ x &= x + x_{off} + \sigma_x N \end{aligned} \tag{34}$$

N is a normally distributed random number with zero mean and unit variance. This model incorporates six error parameters. The coordinate offset x_{off} represents positioning error, (for example an error in locating the component on the translation stage). The coordinate fluctuations σ_x represents errors in the motion of the beam. The offset errors in the beam function parameters Γ_{off} and ω_{off} represent the inaccuracy in the experimental determination of these parameters. Fluctuations of these parameters σ_Γ or σ_ω could be caused by power fluctuation and random deviations from the ideal beam shape. Each of the six error parameters are evaluated separately, whereas the others are set to zero.

In this section, we explore the sensitivity of the model to these error parameters. All simulations use an expansion of order $k = 3$. The simulations are first run with no errors, to indicate the baseline results shown in *Table 2.* In both cases, the figuring to a flat and a spherical contour, the sample is figured to 47 nm rms deviation from the desired figure. This is the theoretical limit of the process directly related to the accuracy of the function fit chosen for the desired removal. If the expansion order is increased, the theoretical limit could be reduced. Therefore, for the ideal case, the final figure error is equal to the error of the original fit to the removal map. The improvement is the amount the figure error was reduced. On all the plots, the initial figure error is shown for both the flat and the spherical case.

Figure 2A shows the resulting final rms figure error versus the modeled beam width ω. The offset error in the beam width was varied from -5 to 5 mm. The solution was performed for a beam width $\omega_0 = 10$ mm with zero offset. Therefore, the ideal figures ($\zeta_f = 47$ nm rms) are at $\omega = 10$ mm. The plot shows that the workpiece figure is not improved if the actual beam width is greater then 14 mm. If the

Table 2 Results of simulations with no errors

Test case	Initial ξ_i	Fit η	Final ξ_f	Improvement $(\xi_i - \xi_f)$
Flat	234 nm	47 nm	47 nm	187 nm
Sphere	114 nm	47 nm	47 nm	67 nm

actual beam width is less than 10 mm, the improvement decreases fairly linearly to zero improvement, at zero beam width. *Figure 2B* shows the resulting final rms figure error versus the variance of the random beam width error σ_ω. Normally distributed, random errors in the beam width below 3 mm show little effects, but for values above 3 mm, the process no longer produces coherent removal, and no improvement in figure is obtained.

The resulting final rms figure error versus the modeled beam peak removal rate Γ is depicted in *Figure 3A*. In this plot, offset errors in the rate are considered ranging from -100 to 100 nm/min. The best result, minimum figure error, occurs at zero offset where $\Gamma = 100$ nm/min, which was used in the calculation of the solution. The plot shows a symmetric reduction of performance as the removal rate is varied. *Figure 3B* shows the effects of random errors in beam peak removal σ_Γ. As apparent in the plot, these normally distributed fluctuations do not significantly affect the process.

Figure 4A shows the resulting rms figure error versus the position offset (accuracy of locating the part with respect to the ion beam). The plot shows the reduction in performance as the location accuracy is decreased. From these data, the process does not seem to be significantly affected if the beam is position within 10 mm of the expected relative location. *Figure 4B* shows the resulting rms figure error versus a normally distributed random position error. The random errors seem to cause a more detrimental effect at first. However, it should be noted that the random errors inherent in the

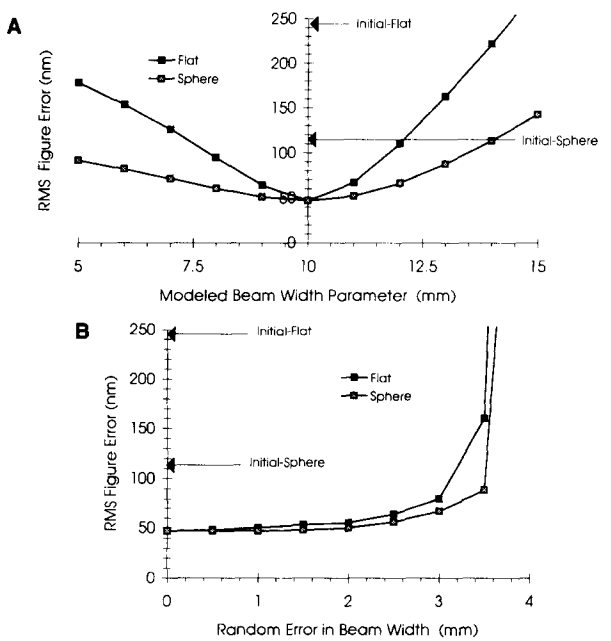

Figure 2 (A) The resulting final rms figure error versus the modeled beam width ω (solution performed for beam width $\omega_0 = 10$ mm). (B) The resulting final rms figure error versus the variance of the random beam width fluctuation error σ_ω

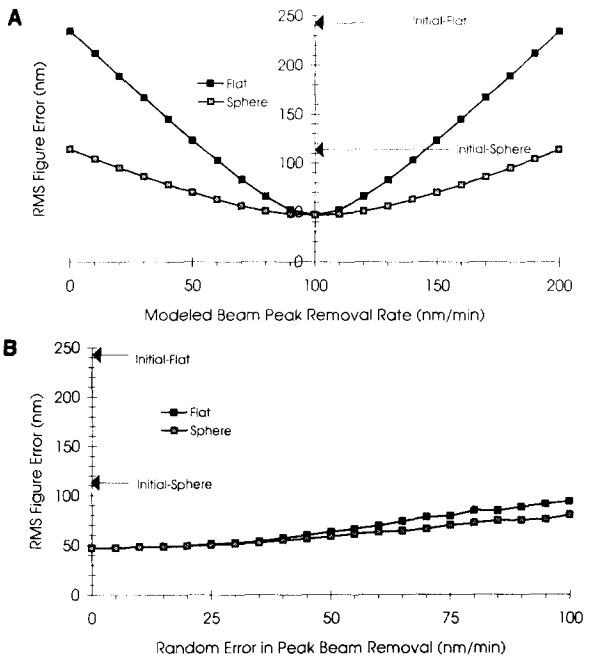

Figure 3 (A) The resulting final rms figure error versus the modeled beam peak removal Γ (solution performed for beam peak $\Gamma_0 = 100$ nm/min). (B) The resulting final rms figure error versus the variance of beam peak removal fluctuation error σ_Γ

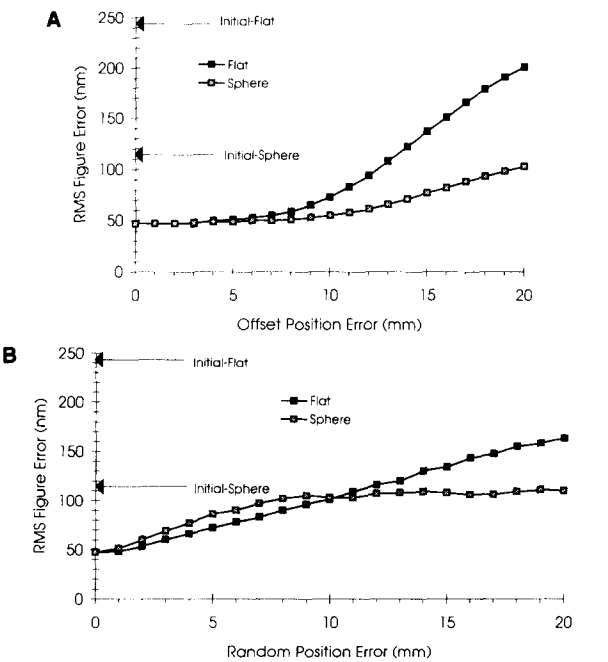

Figure 4 (A) The resulting rms figure error versus the position offset x_{off}. (B) The resulting rms figure error versus the variance of the random position error σ_x

system are of a lower magnitude than the static positioning errors of *Figure 4A*. The random errors that would occur will be related to beam variances and translational stage movements and can be

maintained well below the 1-mm point where they begin to cause significant figure errors. The ion beam is spatially stable during the process, and the stage accuracy is well below the 1-mm threshold.

The simulations of *Figures 2, 3,* and *4* show two cases: a flat and a sphere. It is useful to generalize the results for *Figures 2* and *4,* where the ordinate of the plots (resulting figure error) is normalized. This normalization gives a resulting percentage of the difference between the initial figure error and the ideal surface (which is the error of the original fit to the removal map) and is defined below as a *performance factor.*

$$\xi = \frac{\zeta_i - \zeta_f}{\zeta_i - \eta} \tag{35}$$

The abscissa is normalized in a similar manner by taking a ratio of the given dimension with respect to the beam width. The plots are used to determine the relationship of the parameters to the potential process results for a generic optical contour. The generalized information from the normalized plots is applicable to any target scale and expected beam profile. The results of this normalization are shown in *Figures 5* and *6.* In these plots, the two cases show very similar behavior.

Fitting order k

The effectiveness of the series expansion for the removal function is critical to the performance of the machining system. The solution provided by the algorithm assumes that the series expansion represents the surface contours sufficiently. The resulting function for the dwell function is an *exact* solution. The resulting figure will be no more accurate then the fit of this solution to the removal map. This fitting of the series expansion to the removal is the only computationally difficult and time-consuming step. It is important to determine the most efficient process for fitting the expansion, including the minimum number of terms necessary to represent a surface accurately.

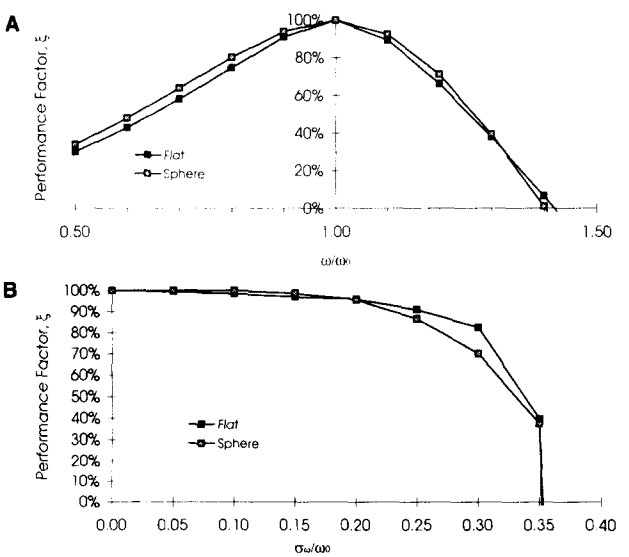

Figure 5 (A) Normalized plot of constant beam width error. (B) Normalized plot of fluctuating beam width error

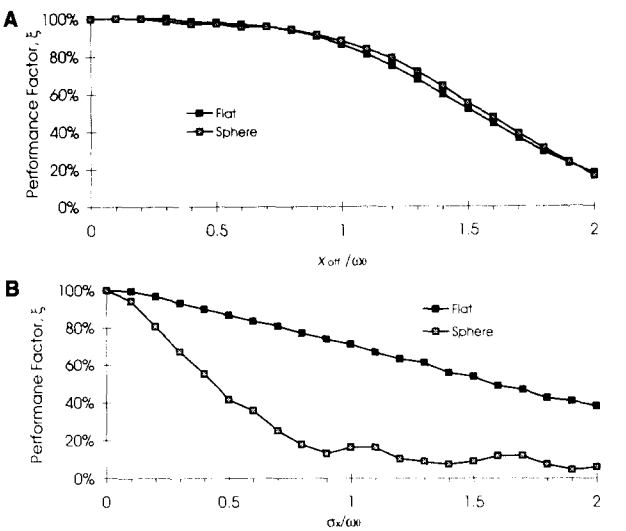

Figure 6 (A) Normalized plot of constant position error. (B) Normalized plot of fluctuating position error

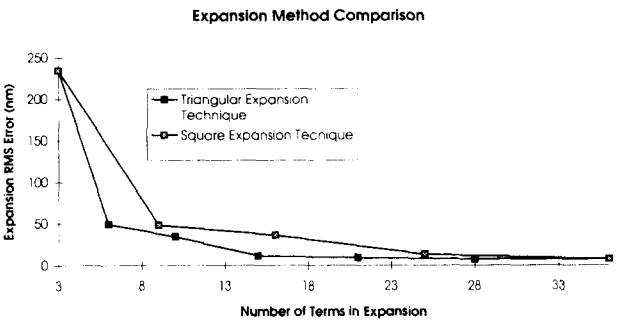

Figure 7 The *goodness-of-measure* η compared to the actual number of terms for the two expansion methods.

Previously, the fitting order k in the series expansion was the highest individual order in the orthogonal spatial dimensions. An expansion of order k has a $k \times k$ square array of coefficients with k^2 terms. This is denoted as a square expansion. Another way of interpreting k is as the highest total order in x and y. The technique is a triangular expansion of order k. The expansion in Equation (16) would then become as follows.

$$R(x,y) = \sum_{l=0}^{k} \sum_{m=0}^{k-1} a_{lm}\, \phi_{lm}(x,y) \tag{36}$$

This method has a triangular array of coefficients and the number of terms in the expansion is equal to

$$\sum_{n=1}^{k} n.$$

Figure 7 shows the results of fitting the two expansion techniques to the removal map compared to the actual number of terms (data points are taken for $k = 1, 2, \ldots$). As apparent in the plot, the triangular expansion converges much faster. This means that fewer terms are necessary; the computations are faster and hence are more stable. In all future algorithms, the triangular expansion is used.

It is desirable to keep the expansion order k as low as possible for efficiency. It is meaningless to fit the surface to higher accuracy than that provided by the metrology. The higher the number of terms, the longer the computation takes and the less stable a fitting routine becomes. Additionally, solutions to higher-order expansions include high-frequency behavior as the expansion corrects for random fluctuations between datapoints. This behavior does not represent most actual desired optical surfaces, and the broad-team ion-figuring process is not capable of generating high-frequency shapes.

Figure 8 shows the goodness-of-fit compared to the total number of terms in the series expansion up to 100 terms. The plot shows rapid convergence to 10 nm rms at 15 terms and then much slower convergence after 15 terms. The slight discontinuity in the plot around the 10-term expansion is related to the spatial characteristics of the measured surface profile and is not a function of the technique. Theoretically, the fit will converge to zero at some higher number of terms (in practice this would be truncated by the precision of the numbers used in the computer code.) In this example, the surface map was taken from a ZYGO Mark IV interferometer with a physical limit on the measurement accuracy. The noise floor expected from this metrology system is $\lambda/50$ or 12 nm ($\lambda = 632.8$ nm). The bend in *Figure 8* is, therefore, corroborated by the accuracy of the metrology system. For this surface, 15 terms can sufficiently characterize the figure.

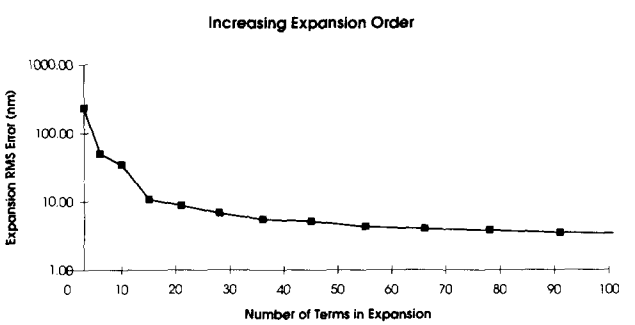

Figure 8 The *goodness-of-measure* η as a function of the total number of terms in the series expansion.

In these operations, the workpiece is measured and then fit by the triangular expansion. If there is more than 12 nm rms (the accuracy of the metrology) difference between the surface map and the polynomial expansion ($\eta \geq 12$ nm), the fit is repeated with a higher-order expansion. In actual operation, the order is repeatedly increased until no significant improvement in the fit is demonstrated. It is expected that the number of terms needed will be on the order of 15 ($k = 5$). Computations for this number of terms are very fast and efficient. Also, no difficulties have been experienced regarding the stability of the fitting algorithms.

Conclusion

The new precision ion machining system research facility at NASA's Marshall Space Flight Center is focused on the figuring of small (≅10-cm diameter) optical mirrors. The surface profile measurements are taken using a ZYGO Mark IV interferometer. The surface roughness measurements are taken using a WYKO three-dimensional optical surface profilometer. The ion-machining apparatus itself is constructed around a surplus sputtering vacuum chamber. Fitted inside the chamber is a 3-cm, Kaufman filament-type ion source driven by a programmable power supply. A computer-controlled translation stage is fitted to the floor of the chamber. The optical components are attached to a special holder designed to facilitate transfer of the component between the metrology equipment and the machining apparatus. The holder is placed on the translation stage that provides translations and rotations of the optic. The stage has 100-mm range and 360° rotation at speeds up to 15 RPM. The motion of the system as well as the ion source power supply will be controlled by a 80386-based personal computer. In this setup, the workpiece is moved, and the ion beam source is held in a fixed position.

The process of figuring an optical component involves the following steps. The component's surface profile is measured on the interferometer, and the surface height data map is transferred to the controlling PC. The surface data are loaded into the targeting program, and the desired contour and the order of the functional expansions are chosen. The targeting program reports the initial rms deviation from the desired profile ζ_i and indicates the accuracy of the function fit to the desired removal η. If the fit is sufficiently accurate $\eta \leq 12$ nm, the program computes the solution for the dwell function. The component is positioned in the chamber and brought under vacuum. An appropriate machining path is chosen for the process. The targeting program activates the ion beam and rasters the component following the paths at velocities determined by the dwell function. When the process is complete, the optical component is removed and evaluated for both surface figure and resulting surface

finish. The final figure data are transferred to the controlling PC, and the program reports the final rms deviation from the desired contour ζ_f.

The data obtained from the simulation work provide operational guidelines for the ion-machining process. These data will be utilized in the design of support hardware and processing procedures for future experiments in the PIMS facility. Several optical component samples were acquired for the experimental testing. These include four chemically vapor deposited silicon carbide (CVD SiC) samples and ten fused silica samples. All components have been polished flat and are 80-mm in diameter. The fused silica represent a common material for optical components and will be used to baseline the process. For precision space-based components, CVD SiC could replace the more common glasses because of its inherent toughness, stiffness, and large *critical-depth-of-cut* with regard to damage-free machining. Dissimilar to glass, CVD SiC can be easily ground in an entirely ductile regime.[17,18] Moreover, it has been demonstrated that CVD SiC can be ground with surface finishes of ≅10 angstroms without inducing subsurface damage. Previous research has shown that subsequent ion machining does not significantly degrade the surface roughness of these ductile ground specimens.[11] These future experiments will be used to validate the ion-machining technique by applying the algorithms developed in this paper.

Acknowledgments

This work was sponsored by NASA, and the authors express their gratitude to the following people for their support of the project: Robert Rood, James Bilbro, Charles Jones, and Joseph Randall. We also recognize the insight and inspiration provided by Guido Sandri and Raymond Nagem. We particularly appreciate the open and informative assistance of other researchers in this area: Scott Wilson, Lynn Allen, and Charles Egert, and we thank them.

References

1 Allen, L. N., Hannon, J. J. and Wambach, R. W. "Final surface error correction of an off-axis aspheric petal by ion figuring," in *Advances in Fabrication and Metrology for Optics and Large Optics,* Bellingham, WA: SPIE, 1991, p. 1543

2 Allen L. N. and Keim, R. E. "An ion figuring system for large optics fabrication," in *Current Developments in Optical Engineering,* Bellingham, WA, SPIE, 1989, p. 1168

3 Allen, L. N., Kiem, R. E. and Lewis, T. S., "Surface error correction of a Keck 10m telescope primary segment by ion figuring," in *Advances in Fabrication and Metrology for Optics and Large Optics,* Bellingham, WA, SPIE, 1991, p. 1531

4 Allen L. N. and Romig, H. W., "Demonstration of an ion figuring process," in *Advances in Fabrication and Metrology for Optics and Large Optics,* Bellingham, WA, SPIE, 1990, p. 1333

5 Wilson, S. R., "Ion beam figuring of optical surfaces," Master's thesis, University of New Mexico, 1987

6 Wilson, S. R. and McNeil, J. R., "Neutral ion beam figuring of large optical surfaces," in *Current Developments in Optical Engineering,* Bellingham, WA, SPIE, 1987, pp. 320–323

7 Wilson, S. R., Riecher, D. W. and McNeil, J. R., "Surface figuring using neutral ion beams," in *Advances in Fabrication and Metrology for Optics and Large Optics,* Bellingham, WA, SPIE, 1988, 74–81

8 Kaufman, H. R., Reader, P. D. and Isaacson, G. C., "Ion Sources for Ion Machining Applications," *AIAA J,* 1977, **15,** 843–847

9 Gale, A. J., "Ion Machining of Optical Components," Optical Society of America Annual Meeting Conference Proceedings, Nov. 1978

10 Carnal, C. L., Egert, C. M. and Hylton, K. W., "Advanced matrix-based algorithm for ion beam milling of optical components," paper presented at the Society of Photo-Optical Instrumentation Engineers, 1992 International Symposium on Optical Applied Science and Engineering, 1992

11 Fawcett, S. C., Drueding, T. W. and Bifano, T. G., "Neutral Ion Figuring of CVD SiC," *Opt Eng,* 1994, **33,** 967–974

12 Jansson, P. A., *Deconvolution: With applications in spectroscopy.* Orlando, FL: Academic Press, 1984

13 Eddington, "On a formula for correcting statistics for the effects of a known probable error of observation," *Mon Not R Astron Soc,* 1913, **73,** 359–360

14 Hohlfeld, R. G., King, J. I. F., Drueding, T. W. and Sandri, G. v. H., "Solution of convolution integral equations by the method of differentiation inversion," *SIAM J Appl Math,* 1993, **53**

15 Bochner, S. and Martin, W., *Several complex variables.* Princeton University Press, Princeton, NJ, 1948

16. Press, W. H., Flannery, B. P., Teukolsky, S. A. and Vetterling, W. T. *Numerical Recipes in C,* Cambridge University Press, Cambridge, UK, 1988

17 Bifano, T. G. and Fawcett, S. C., "Specific grinding energy as an in-process control variable for ductile-regime grinding," *Precision Engineering,* 1991, **13,** 256–262

18 Bifano, T. G., Yi, Y. and Kahl, W. K., "Fixed abrasive grinding of CVD SiC mirrors," *Precision Engineering,* 1994, **16,** 109–116